Journal of Power Sources 181 (2008) 186–192

Contents lists available at ScienceDirect

Journal of Power Sources

journal homepage: www.elsevier.com/locate/jpowsour

Electrochemical and capacitive properties of thin-layer carbon black electrodes

V.V. Panić, R.M. Stevanović, V.M. Jovanović, A.B. Dekanski*

Institute of Chemistry, Technology and Metallurgy – Department of Electrochemistry, University of Belgrade, Belgrade, Serbia

ARTICLE INFO

Article history:
Received 8 December 2007
Received in revised form 16 February 2008
Accepted 21 March 2008
Available online 28 March 2008

Keywords:
Carbon black
Electrochemical supercapacitors
Double-layer capacitance
Pseudocapacitance
Electrochemical impedance spectroscopy (EIS)

ABSTRACT

Electrochemical properties and porous-structure-dependent capacitive ability of commercial carbon blacks, Black Pearls 2000® (BP) and Vulcan® XC 72R (XC), were investigated in H_2SO_4 solution by cyclic voltammetry (CV) and electrochemical impedance spectroscopy (EIS). The capacitance in-depth profile is correlated to microscopic appearance of carbon blacks in the form of a thin layer applied over Au substrate from water suspensions of BP and XC. The capacitance calculated from voltammetric charge was found to depend on the sweep rate, due to porosity of investigated materials. Impedance (EIS) characteristics upon frequency-dependent charge/discharge process indicate transmission line electric behavior of BP and XC. Capacitance and resistance values obtained by simulations of EIS data, enabled estimation of capacitance and resistance profile throughout carbon black porous electrodes. Capacitance of BP carbon layer increases going from the outer surface towards the bulk of the layer. External capacitance originates from capacitive characteristics of the macroscopic surface consisting of relatively large agglomerates, while internal capacitance originates from "inner" surface of micro-porous agglomerates. Contrary to BP, opposite distribution of the total capacitance to external and internal part was found for XC, caused by its loose structure and considerably lower real surface area in comparison to BP. The XC morphology makes additionally the pseudocapacitive contribution of surface functionalities more pronounced, which indirectly shifts also the "internal" double-layer capacitive response to higher frequencies through the effect of increased wettability of the layer. Thus, the capacitance of XC surface directly exposed to the electrolyte is larger than that of the inner one, which makes it a "fully-utilized" capacitor, while increased capacitive performance of BP emerges only at very low frequencies of charging/discharging process.

1. Introduction

Electrochemical supercapacitors (ECS) have been investigated over many years due to their energy and power density capabilities bridging the gap between batteries and classical electric capacitors [1,2]. Energy storage mechanism of ECS arises not only from charging of electrochemical double layer (EDL supercapacitors) at the electrode/electrolyte interface, which is the dominant charging mechanism of high surface area carbons [3], but also from pseudocapacitance involving reversible Faradaic charge transfer reactions (conductive polymers, noble metal oxides and partially carbons) [1]. For this reason, wide variety of carbon-based materials [4], like carbon blacks [5–8], carbon fibres [9–11], cloths [12] and nanotubes [13,14], as well as glassy carbon [15], have attracted attention due to the ease of nano-technology processing that leads to high surface area, high porosity and consequently, to high power density [3,16–18,14,19–21]. Additionally, due to affinity to form composites, carbon materials are extensively investigated as catalyst support [22–30].

Specific capacitances larger than 300 F g^{-1} can be achieved with carbon black materials of highly developed surface (>1000 m^2 g^{-1}) and 15-nm particles grouped in up to 200-nm sized agglomerates [6,31,32]. The porous structure of these materials may include micro- (<2 nm), meso- (between 2 and 50 nm), and macro-pores (>50 nm), which act differently as supplier of the electrolyte to the inner surface of porous material [6,21]. This part of the surface is hardly accessible and its contribution to the capacitive response is limited by the type of electrolyte used [19,20,33–37]. In addition, electroactive functionalities at the carbon surface also contribute to overall capacitive performance with their pseudocapacitance associated with redox processes [33,38].

In composite materials, high surface area carbons improve the pseudocapacitive charge/discharge behavior of noble metal oxides, such as RuO_2 [39,40]. The role of carbon in the composite is to disperse oxide material, which enhances oxide capacitive utilization. It was found that morphology, chemical properties and capacitive

* Corresponding author. Tel.: +381 113640231; fax: +381 113640234.
E-mail address: dekanski@ihtm.bg.ac.yu (A.B. Dekanski).

0378-7753/$ – see front matter © 2008 Elsevier B.V. All rights reserved.
doi:10.1016/j.jpowsour.2008.03.048

characteristics of the composite materials are influenced by the structure of carbon blacks [39–47].

From these considerations, it appears as crucial a detailed understanding of the electrochemical performance of commercial carbon blacks as the support of electrocatalysts and pseudocapacitive materials, in connection to desired activity and/or energy–power density relationship. Qu and Shi [33] investigated capacitive performance of variety of high-surface-area carbon blacks in the form of a sheet. They found excellent correlation between transmission-line *ac* behavior and BET pore distribution characteristics. However, no significant difference in *RC* distribution between various carbon blacks was found since for all of them surface areas were rather high (above 1200 $m^2\,g^{-1}$). On the other hand, specific capacitances did not exceed 100 $F\,g^{-1}$ which indicates that rather large amount of internal surface remained inaccessible during *ac* charge/discharge experiments. Similar result was also reported by Raimondi et al. [48]. However, the influence of carbon morphology on the number of elements in the transmission-line model is usually neglected (due to rather high real surface area) [20,33,38,49,50]. Also, it is not clear how the different contribution of surface functionalities influences the constitution of equivalent electrical circuit, while it is straightforwardly depicted that gathering of primary particles into agglomerates can affect the capacitive performance of the material.

Having in mind above considerations, capacitive response of as-received commercial carbon blacks, Black Pearls® 2000 (BP) and Vulcan® XC-72R (XC), were investigated in the form of a thin layer in this work. The thin layers are expected to show an enhancement of electrolyte accessibility to the internal surface of the layer, thus giving a real picture of capacitive performance during a real-time power demands. Electric equivalents of thin layers, according to *ac* impedance measurements in H_2SO_4 solution, are discussed in correlation to morphology and cyclic voltammetry behavior. The results are expected to help in estimation of capacitance and resistance profile across carbon black porous electrodes from the standpoint of desired application as catalyst support, power suppliers and memory backups.

2. Experimental

The carbon blacks investigated, BP and XC, both from CABOT Corporation, Canada, were used as received. According to the literature data BP and XC carbons expose BET surface areas of 1475 and 248 $m^2\,g^{-1}$, respectively [4].

The working electrodes were formed from BP and XC water suspensions onto Au and glassy carbon substrates as current connectors, in the form of rotating disk electrode. However, it was registered that the material of the substrate does not affect capacitive properties of subsequently formed BP and XC layers. This was also observed in previous works [32,46,47] when differently prepared C/RuO_2 composites were electrochemically investigated. Hence, the type of the substrate will not be explicitly denoted in forthcoming text.

The layers were formed by pipetting the ultrasonically homogenized aqueous suspension of carbon black (3 $mg\,cm^{-3}$), in the quantity of 30 $\mu l\,cm^{-2}$, onto the rotating disk substrates. The applied suspensions were left to dry in the air at room temperature. In order to preserve the dried carbon black layer from being detached in contact with electrolyte, it was covered with a thin Nafion® layer. The 10:1 (v/v) mixtures of 18 MΩ water and commercial Nafion® solution (in ethanol, 5% mass, 1100 E.W., Aldrich) were applied in the quantity of 30 $\mu l\,cm^{-2}$. The electrode assembly was air-dried again for about 12 h.

Cyclic voltammetry (CV) measurements were performed in 0.5 mol dm^{-3} H_2SO_4, at room temperature in a three-compartment cell equipped with Pt-mesh counter electrode and saturated calomel electrode (SCE) as the reference electrode. The cyclic voltammetry experiments were performed using a PAR Model 273 potentiostat and Philips Model 8033 X-Y recorder.

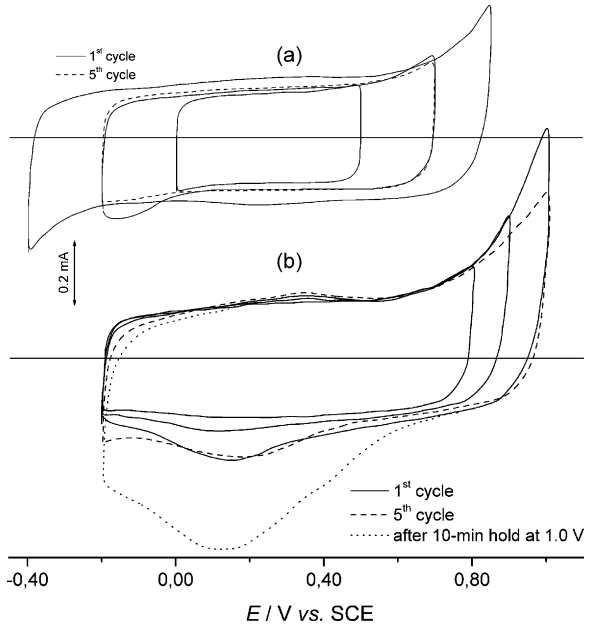

Fig. 1. Influence of the potential limits on the CV characteristics of BP carbon black in 0.50 mol dm^{-3} H_2SO_4: (a) non-deaerated and (b) deaerated solution. Scan rate: 20 mV s^{-1}.

Electrochemical impedance spectroscopy (EIS) experiments were performed in 0.5 mol dm^{-3} H_2SO_4 around the potential of 0.55 V, in the 0.50 mol dm^{-3} H_2SO_4. The working potential was chosen according to detailed CV measurements that indicate Instrumentation involved GAMRY® Instruments Femtostat, model FAS32, guided by Gamry Framework® software. The working electrode responded to the potential input sinusoidal signal of ±10 mV (rms) amplitude. Experimental EIS data were fitted by ZView® software [51].

Experiments were conducted at room temperature (20–25 °C). All the reagents used were of p.a. grade, and the solutions were prepared with 18 MΩ water. The electrolytes were purged with nitrogen before every experiment, if not stated differently.

Surface morphology of the electrodes was examined by scanning electron microscopy (SEM) using JEOL microscope, model JSMT20 (U_w = 20 kV).

3. Results and discussion

3.1. CV potential window of carbon black cycling stability

Cyclic voltammetry behavior of prepared BP thin layer in H_2SO_4 solution is demonstrated in Fig. 1. The influence of the successive extension of cycling limits towards potential window of electrolyte and/or carbon stability on the shape of voltammetric curve in non-deaerated solution is shown in Fig. 1a, while Fig. 1b shows the influence of the successive extension of anodic cycling limit up to the onset of oxygen evolution in deaerated solution.

The CV shape and voltammetric currents do not change upon cycling in the potential range between 0 and 0.50 V (Fig. 1a). Rectangle-like shape of CV implies that BP carbon black, in this potential range, behaves like double-layer capacitor. If lower cycling limit is set to −0.20 V and upper to 0.70 V in subsequent scan (Fig. 1a), broad current peak appears in the cathodic part of the first

cycle at the potential of—0.15 V, while the anodic currents start to increase at about 0.60 V. Also, voltammetric currents are larger than those obtained upon potential cycling in the double-layer region (from 0 to 0.50 V). Intensity of the broad cathodic peak decreases with cycling, and almost disappears after the fifth cycle (dashed line in Fig. 1a). The increase in anodic currents, seen in first cycle in the potential range from 0.60 to 0.70 V, becomes less pronounced after the fifth cycle. However, the cathodic current peak at—0.15 V can be completely recovered if the electrode is subjected to the rotation (not shown). In addition, this peak was not detected in deaerated solution (Fig. 1b). These observations suggest that cathodic current peak at—0.15 V can be attributed to the reduction of dissolved oxygen.

When cycling limits shift to −0.40 and 0.85 V after oxygen exhaustion from the near-electrode layer by cathodic reduction (five cycles in the range −0.20–0.70 V), anodic currents still increase in the potential range from 0.60 to 0.85 V, while cathodic currents increase from the potential of about −0.20 V (Fig. 1a), which corresponds to the onset of hydrogen evolution [52]. Overall voltammetric currents are higher in comparison to those registered in narrower potential ranges, with additional modest appearance of a broad reversible current peak near the potential of about 0.30 V. Maruyama and Abe [53] registered redox current peaks at potential of about 0.60 V_{RHE} before and after the anodic activation of glassy carbon, which they assigned to quinone/hydroquinone (Q/H_2Q) redox couple. Appearance and intensification of the Q/H_2Q redox couple upon anodic activation of carbon black electrode materials is the consequence of continuous formation quinonic surface groups [53,54–56]. Thus, the modest appearance of redox couple upon cycling in the potential range from −0.40 to 0.85 V (Fig. 1a), can be assigned to the quinonic groups formed at the surface of carbon particles during anodic excursions above 0.60 V. It should be mentioned here that Q/H_2Q redox couple is poorly pronounced (Fig. 1a) if compared to that obtained with anodic activation of glassy carbon (GC) [25] due to short potentiodynamic activation at moderate anodic potentials. Additionally, BP real surface area is considerably larger, hence non-Faradaic double-layer charging/discharging currents are much larger in comparison to that of Q/H_2Q redox transition.

If anodic cycling limit is set to 0.90 V, Q/H_2Q redox transition becomes more pronounced (Fig. 1b). Additional extension of the anodic cycling limit up to the 1.0 V leads to more pronounced increase of the cathodic current peak than the anodic one (Fig. 1b). Anodic voltammetric currents in the potential range from 0.80 to 1.0 V decrease upon cycling, while intensity of the cathodic current peak does not change (dashed line, Fig. 1b). This suggests that some irreversible reduction process may take place after anodic activation up to 1.0 V. Sullivan et al. [54] found that carbonyl and carboxyl groups are formed during anodic activation and reduced in the subsequent cathodic potential scan.

If the potential hold is performed at the anodic cycling limit of 1.0 V, the subsequent cathodic scan reveals intensification of the cathodic current (dotted line, Fig. 1b). In the next scan cycle (not shown), intensity of the hold-induced peak subsides to the value obtained during the cycling before the potential hold. Therefore, anodic voltammetric currents in the potential range from 0.80 to 1.0 V comprise those related to the formation of oxygen-containing surface groups, which reduction is registered at the potential of about 0.15 V.

3.2. Sweep rate-dependent voltammetric features of BP and XC

Cyclic voltammograms of BP thin-layer electrode, obtained in deaerated H_2SO_4 solution at different potential sweep rates, are shown in Fig. 2a. Q/H_2Q redox couple is most pronounced at the lowest sweep rate of 5 mV s^{-1}. This redox transition is less pronounced at higher sweep rates since non-Faradaic double-layer charging/discharging current increases with sweep rate. Also, the irreversible cathodic peak can be seen at about −0.05 V, and only at the lowest sweep rate, which is related to reduction of surface oxygen-containing groups. At higher sweep rates this current peak is absent, due to insufficient duration of anodic activation and partly because it is overcome by double-layer discharging currents.

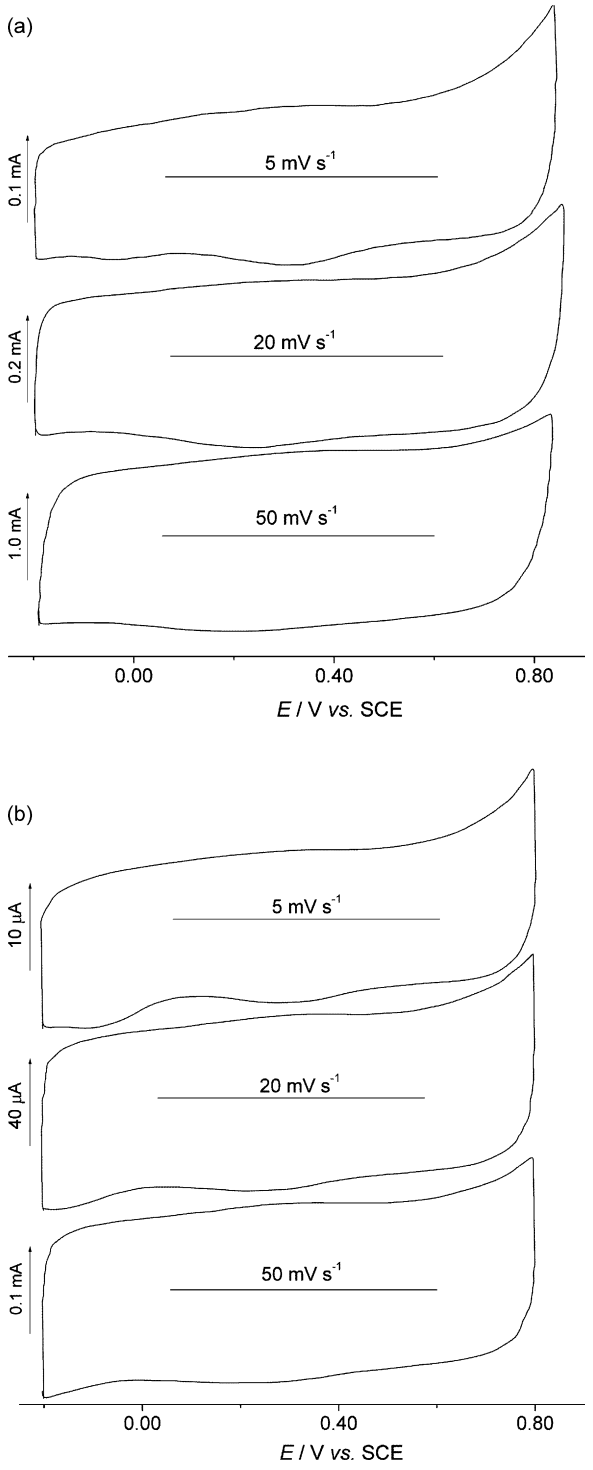

Fig. 2. Cyclic voltammograms of (a) BP and (b) XC carbon black thin-layer electrode in deaerated 0.50 mol dm^{-3} H_2SO_4 at different sweep rates.

Table 1
The values of characteristic specific capacitances of BP and XC carbon blacks

Capacitance ($F g^{-1}$)	Electrode	
	BP	XC
C_T	310	27
C_S	43	16
C_U	267	11

Similar CV characteristics at different sweep rates in deaerated H_2SO_4 solution are registered for XC thin-layer electrode. These are shown in Fig. 2b. Q/H_2Q redox couple is observed around 0.30 V, while cathodic irreversible current peak appears at −0.05 V, as in the case of BP. Contrary to BP, the cathodic current peak may be seen even at high sweep rates. However, currents are ten-fold lower for XC electrode. These differences between XC and BP electrode are result of significantly lower real surface of the XC electrode.

As expected for porous media [57], charge spent for voltammetric charging/discharging process at carbon black thin-layer electrodes was found to depend on the sweep rate, v. Dependence of voltammetric charge, as well as of the capacitance, C, on v is commonly explained by the existence of hardly accessible internal surface within the porous medium. An increase in v causes internal surface to be more and more excluded from charging/discharging. Ardizzone et al. [57] showed that dependence of capacitance on the sweep rate can be expressed by following equations:

$$C = C_S + \frac{k}{\sqrt{v}} \quad (1)$$

and

$$\frac{1}{C} = \frac{1}{C_T} + k'\sqrt{v} \quad (2)$$

where C stands for the capacitance at sweep rate, v, while k and k' are constants. Capacitance C_S is the capacitance of external surface, which is directly exposed to the electrolyte, while C_T is total capacitance of the porous layer. Assuming that Eqs. (1) and (2) lead to:

$$C \to C_S \quad \text{if } v \to \infty \quad (3)$$

and

$$\frac{1}{C} \to \frac{1}{C_T} \quad \text{if } v \to 0 \quad (4)$$

total and external surface capacitances, C_T and C_S, could be estimated by extrapolation of linear C vs. $v^{-1/2}$ and C vs. $v^{1/2}$ to zero, i.e., to infinite and zero sweep rates, respectively. The difference between C_T and C_S corresponds to the capacitance of internal surface of the porous layer, C_U:

$$C_U = C_T - C_S \quad (5)$$

The values of characteristic specific capacitances expressed per unit mass of the porous layer, determined from cyclic voltammograms and Eqs. (1–5), are shown in Table 1. Taking into account literature data for BET specific surface area of the BP and XC carbon blacks and obtained value for total capacitance C_T, capacitances of BP and XC normalized to the unit surface area are 21 and 11 $\mu F\,cm^{-2}$, respectively. These values are in good agreement with literature data (10–30 $\mu F\,cm^{-2}$) [4].

Hence, C_T value corresponds to complete utilization of the total real surface of carbon electrodes. In the case of BP carbon, almost 90% of total specific capacitance originates from participation of the internal surface, which contributes only in moderate to slow charging/discharging process. This specific electric behavior of BP can be connected to its morphology.

Typical SEM appearances of the surface of BP and XC thin layers, obtained after evaporation of the dispersing medium, are shown in Fig. 3. BP carbon microstructure is characterized by randomly distributed agglomerates of irregular shape and different sizes, from 10 to 60 μm (Fig. 3a). Crater-like holes with diameter of about 30 μm, which can be denoted as macro-pores, are seen. Typical appearance of an agglomerate surface, shown in Fig. 3b, implies that agglomerates consist of uniform porous particle matrix, with sporadic presence of smaller agglomerates (0.5–1 μm) of blinded particles. The pores of the matrix are uniformly sized and distributed, do not exceeding 150 nm (micropores), which is in agreement with literature data [4,58].

Having in mind morphology of BP carbon layer (Fig. 3a and b) it can be concluded that capacitance C_S originates from capacitive characteristics of the microscopic surface (Fig. 3a) consisting of large agglomerates, while capacitance C_U originates from internal surface of micro-porous agglomerates and particle matrix (Fig. 3b).

Contrary to BP carbon, XC carbon electrodes exhibit opposite distribution of total capacitance to external and internal part of the surface. The fact that, in this case outer surface capacitance is larger than inner capacitance can be explained by the morphology of XC layer (Fig. 3c).

SEM microphotograph of the surface of XC thin layer obtained at the angle of incidence of 30°, which is shown in Fig. 3c, reveals loose structure, with no clearly defined grains or agglomerates. Presence of large number of pores of different shapes and dimensions points to considerably less compact structure comparing to BP carbon. This morphology and low bulk density of XC can facilitate the electrolyte accessibility to the internal surface.

3.3. Electrochemical impedance spectroscopy

Complex plane admittance plots for BP and XC carbon black electrodes, obtained in H_2SO_4 solution at the potential of 0.55 V, are shown in Fig. 4. Overlapped capacitive semicircles are seen for both BP and XC electrodes, but with more pronounced overlapping in the case of the BP carbon electrode. Appearance of capacitive semicircles is a typical indication that system investigated is electrically equivalent to a network of frequency-dependent resistor and capacitor in series, which points to capacitance distribution across the porous layer according to De Levie model [1]. Apart from differences in impedance values, a main dissimilarity in the shape of the admittance plots for BP and XC electrodes is obtained in the low-frequency range (below 10 Hz). While real admittance component of BP decreases with decreasing frequency, with the diagram tending to imaginary axis, the real as well as imaginary admittance component of XC increase with decreasing frequency. These admittance characteristics of XC can be related to resistor and capacitor in parallel.

The shape of admittance plot for XC at low frequencies changes with increasing number of charging/discharging cycles in the potential range from −0.20 to 0.85 V, while successive charging/discharging does not affect admittance characteristics of BP carbon. These changes at low frequencies are seen as somewhat slower increase in admittance than that shown in Fig. 4. This indicates that resistance of a resistor in parallel connection to a transmission line capacitive distribution, which can respond like XC at low frequencies, decreases during successive charging/discharging. Recalling pronounced appearance of current peaks for couple on the voltammograms of XC at the potential around 0.30 V (Fig. 2), resistor in parallel can be attributed to the charge transfer resistance of Q/H_2Q redox transition. Successive charging/discharging of a carbon enhances the formation of surface quinonic groups [55], which produces intensification of Q/H_2Q redox transition current response [53]. Consequently, associated

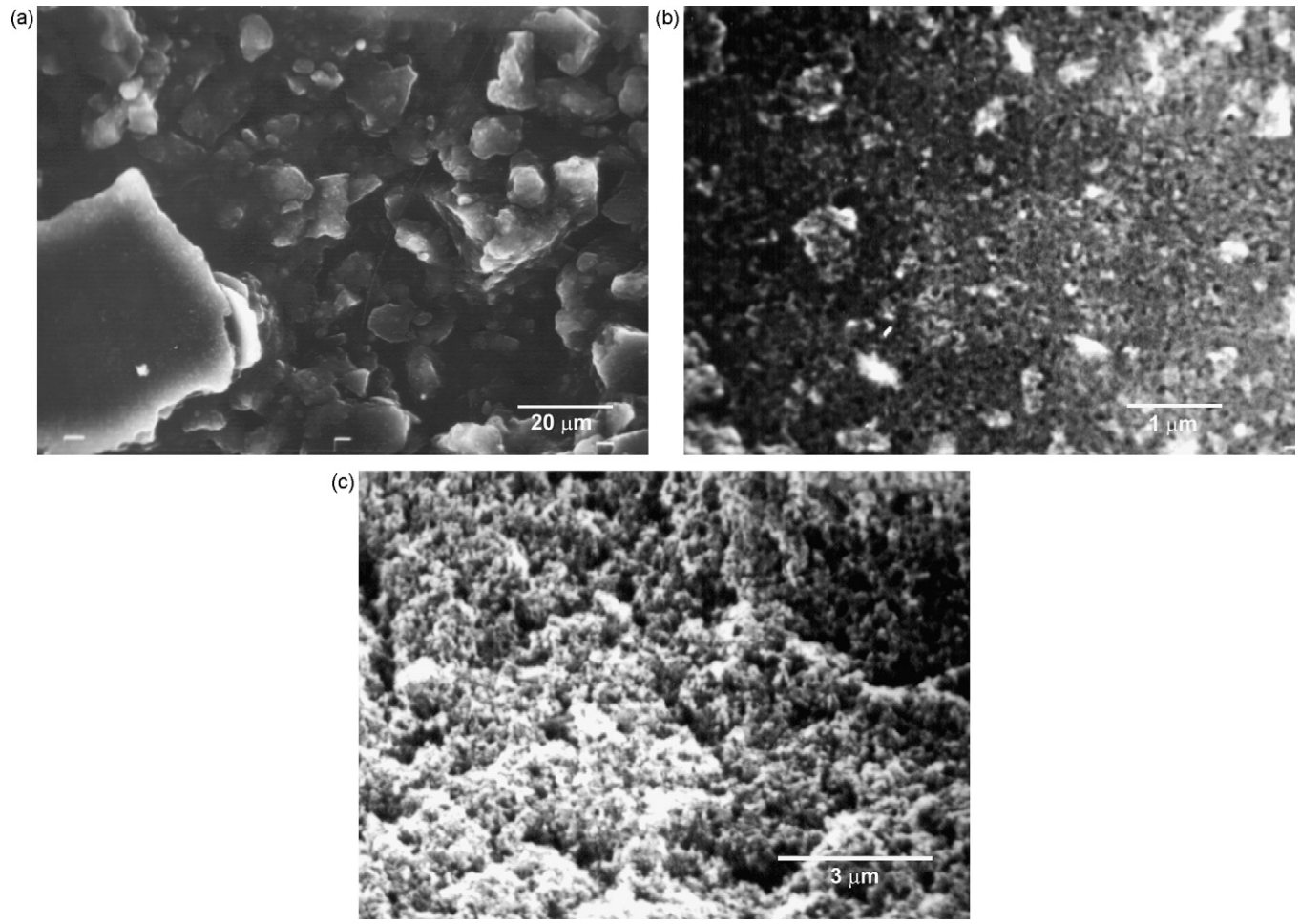

Fig. 3. SEM microphotographs of the surface of thin layers of BP (a and b) and XC (c) carbon blacks.

charge transfer resistance should decrease with prolonged charging/discharging.

Having in mind these qualitative considerations of EIS behavior of BP and XC electrodes, simulation of registered impedance data by equivalent electrical circuits based on transmission line model [1] appeared reasonable. The equivalent electrical circuits which gave the best fitting results (chi-squared based on modulus calculated was below 0.001, while relative error of the parameter values of the elements did not exceed 20%) are schematically presented in Fig. 5, while their EIS responses are given by lines in Fig. 4. A transmission line circuit of the fifth order (i.e., circuit consists of five transmission branches, Fig. 5a) describes best the EIS behavior of BP. For XC, simulation with third-order transmission line in parallel to charge transfer resistance of Q/H_2Q redox transition, R_{pn}, gave the best agreement with experimental data (Fig. 5b). Beside the appearance of the charge transfer resistance in the case of XC, the main difference in electrical equivalents of BP and XC lies in the number of branches representing the capacitance distribution. This difference is in close connection to the morphology of investigated carbon blacks.

Transmission line circuit describes impedance characteristics of a porous layer having the pores of characteristic morphology, with distributed *RC* time constants as a measure of accessibility of different parts of internal surface of a layer. Circuits from Fig. 5 include electrolyte ohmic resistance in the near-electrode layer, R_Ω, and pore resistances, $R_{p,n}$ ($n = 1, 2, \ldots$), related to electrolyte conductivity in the pores. Number of resistors related to pore resistance,

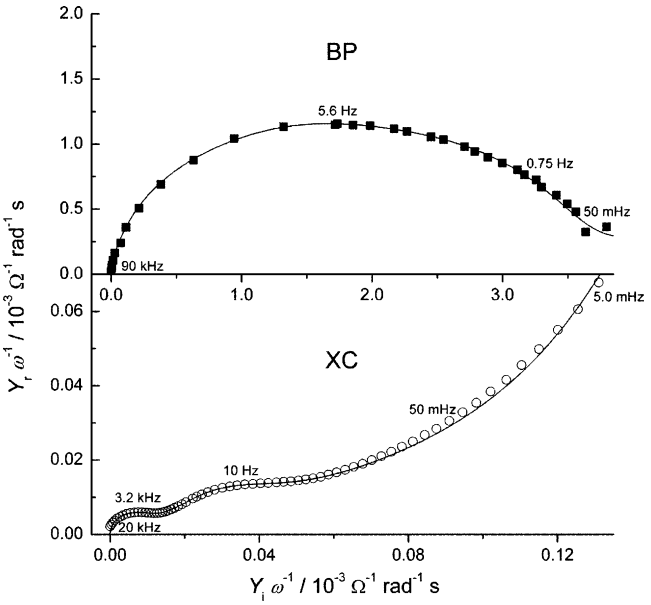

Fig. 4. Admittance complex plane plots of BP and XC carbon black electrodes registered at the potential of 0.55 V_{SCE} in 0.50 mol dm^{-3} H_2SO_4. Fitting results are given by lines.

$R_{p,n}$, in n transmission branches depends on a layer morphology (cross section geometry, equivalent diameter, length and pore tortuosity). Capacitance of the internal surface, available through the pore resistances, are represented by a network of capacitors of the capacitances $C_{U,n}$, or by constant phase elements, $CPE_{U,n}$.

For the transmission line circuit with $(n-1)$ branches containing $R_{p,i}$ and C_i in series and $R_{p,n}$ and CPE_n in nth branch, it can be assumed that the corresponding capacitance is influenced by all preceding resistances [59]:

$$C_n = (Y_{0,n}(R_\Omega + \sum_{i=1}^{n} R_{p,i})^{(1-\alpha)})^{1/\alpha} \quad (6)$$

The physical implication of the Eq. (6) is that the capacitance of the inner coating surface at defined distance l from external surface is electrically accessible only through the cumulative electrolyte resistance in the near-electrode layer, R_Ω, and in the pores of a layer with the depth l, $\sum R_{p,i}$.

In the case of the BP carbon, constant phase element appears only in the last transmission branch (CPE_U, Fig. 5a). This implies that element stands as measure of dimensionality of the entire internal surface.

Structures of applied equivalent circuits, as well as capacitance and resistance values obtained by fitting the experimental EIS data to the circuits, which are supported by the results obtained by SEM and CV measurements, enabled estimation of capacitance and resistance profile throughout carbon black porous electrodes, as shown in Fig. 6.

Starting from the external surface, directly exposed to the electrolyte, (1st branch, $n=1$) towards interior of the BP electrode layer, the increase in capacitance for a two order of magnitude is obtained, which is associated with negligible increase in the pore resistance (down to 3rd branch, $n=3$). However, it should be noted that capacitance in 3rd branch is accessible through $\sum_{i=1}^{3} R_{p,i}$, which is about three-fold higher than the resistances in each branch. Considering BP layer morphology, (Fig. 3a) it can be envisaged that capacitance increases due to the increasing contribution of the part of internal surface, available to the electrolyte through about 30 μm wide macro-pores, as frequency decreases. In the certain frequency range, which corresponds to time constants of 3rd and 4th transmission branches, capacitance values are similar, but pore resistance starts to increase noticeably. Since capacitors are connected in parallel (Fig. 5a), the layer capacitance in this frequency range can be calculated as the sum of capacitances in all preceding circuit branches. This summation down to fourth branch gives the value of 48 F g^{-1} for BP, which agrees with the value for outer capacitance, C_O, obtained by cyclic voltammetry (Table 1). It appears that electrolyte easily reaches those parts of the internal surface

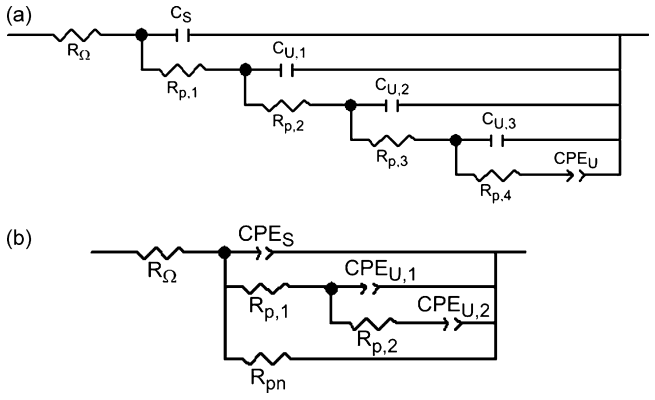

Fig. 5. The most suitable equivalent electrical circuits used to simulate EIS data of BP (a) and XC (b) carbon black electrodes from Fig. 4.

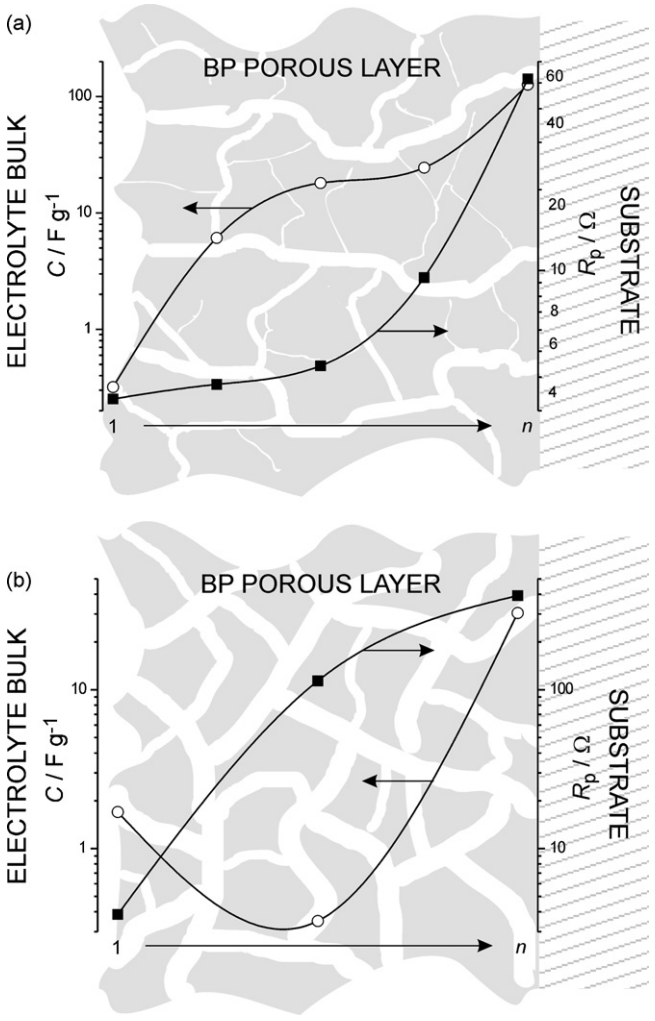

Fig. 6. Capacitance and pore resistance distribution throughout the porous layer of BP (a) and XC (b) carbon black electrodes.

which are available through macro-pores, i.e., space between large agglomerates observed in Fig. 3a.

Near five-fold increase in capacitance as well as pore resistance is registered at sufficiently low frequencies, which correspond to the time constant of the 5th transmission branch. This branch can be associated to the parts of internal surface comprising micro-pores, i.e., micro-porous structure of the agglomerates (Fig. 3b). Total capacitance of the layer equals 175 F g^{-1}, which is nearly two times lower value than that obtained by cyclic voltammetry (Table 1). Having in mind that total capacitance from Table 1 is obtained under hypothetical condition at zero CV charging/discharging rate ($v \to 0$), which, however, corresponds to the BET surface area of BP, it follows from CV and EIS analysis that almost half of the BP thin layer is virtually inaccessible to the electrolyte.

Contrary to BP electrode capacitive in-depth profile, XC carbon capacitance was registered to decrease at moderate frequencies (down to $n=2$) going from the external surface towards the bulk of the layer, with corresponding increase in pore resistance of two orders of magnitude (Fig. 6b). Remarkable increase in capacitance is noticed at very low frequencies, associated with the relaxed increase in pore resistance. It appears that capacitive response of XC internal surface, available through constricted and branched pores of loose XC layer (Fig. 3c), expresses in this low-frequency domain.

Remarkably higher pore resistance as well as the decrease in capacitance going from external towards the interior of the layer

(2nd branch) of XC in comparison to BP carbon could be explained by visually observed poor wetting of XC layer by electrolyte. Similar capacitance distribution to external and internal surface was also obtained from cyclic voltammetry (Table 1). The capacitance of external surface is larger than internal, similarly to EIS data for the first and second transmission line (Fig. 6b). Total capacitance of XC, immediately after electrode immersion, is calculated by summation to be 32.6 F g^{-1}, the value which is in agreement with that obtained by cyclic voltammetry. However, after successive charging/discharging cycles, total capacitance of the layer increases to 39.9 F g^{-1}. This can be explained by the continuous decrease in hydrophobicity of XC layer, as the consequence of carbon activation by formation of surface oxygen-containing groups during prolonged charging/discharging [52].

The similarity of CV and EIS data for XC capacitance profile indicate that this low-surface-area carbon can be nearly completely utilized during slow charging/discharging processes.

4. Conclusion

Capacitance distribution throughout the porous thin layer electrodes of carbon blacks depend on their morphology and real surface area. Capacitance of a layer of high-surface-area carbon Black Pearls 2000® increases going from the external surface towards the bulk of the layer. This increase is associated with negligible increase in pore resistance of the layer. Considerably larger part of the total capacitance of this carbon black originates from its internal surface, which considerable amount is inaccessible to the electrolyte. External capacitance reflects capacitive characteristics of a macro-scale surface consisted of relatively large agglomerates, while internal capacitance originates from inner surface of microporous agglomerates placed deeper in the carbon layer. Contrary to Black Pearls 2000®, low-surface-area carbon black Vulcan® XC 72 R is of loose structure which produces opposite distribution of the total capacitance to external and internal one. In this case, internal surface is fully available for slow charging/discharging processes.

Acknowledgement

This work was financially supported by the Ministry of Science of Republic of Serbia, Contract No. B142048.

References

[1] B. Conway, Electrochemical Supercapacitors—Scientific Fundamentals and Technological Applications, Plenum Publishers, New York, 1999.
[2] R. Kötz, M. Carlen, Electrochim. Acta 45 (2000) 2483–2498.
[3] M.F. Rose, C. Johnson, T. Owens, B. Stephens, J. Power Sources 47 (1994) 303–312.
[4] K. Kinoshita, Carbon-Electrochemical and Physicochemical Properties, Wiley, N.Y, 1988.
[5] J.-B. Donnet, R.C. Bansal, M.-J. Wang, Carbon Black Science and Technology, CRC Press, Boca Raton, USA, 1993.
[6] W. Zhu, D.E. Miser, W.G. Chan, M.R. Hajaligol, Carbon 42 (2004) 1841–1845.
[7] B.M. Babić, B.V. Kaludjerović, Lj.M. Vračar, V. Radmilović, N.V. Krstajić, J. Serb. Chem. Soc. 72 (2007) 773–785.
[8] A.G. Pandolfo, M. Amini-Amoli, J.S. Killingley, Carbon 32 (1994) 1015–1019.
[9] A. Yoshida, I. Tanahashi, A. Nishino, Carbon 28 (1990) 611–615.
[10] I.M. Djordjević, D.R. Sekulić, M.M. Stevanović, J. Serb. Chem. Soc. 72 (2007) 513–521.
[11] B.O. Boskovic, V.B. Golovko, M. Cantoro, B. Kleinsorge, A.T.H. Chuang, C. Ducati, S. Hofmann, J. Robertson, B.F.G. Johnson, Carbon 43 (2005) 2643–2648.
[12] J. Niu, W.G. Pell, B.E. Conway, J. Power Sources 156 (2006) 725–740.
[13] V.V.N. Obreja, Physica E (2007), doi: 10.1016/j.physe.2007.09.044.
[14] D. Tashima, K. Kurosawatsu, M. Uota, T. Karashima, M. Otsubo, C. Honda, Y.M. Sung, Thin Solid Films 515 (2007) 4234–4239.
[15] D. Sun, L. Zhu, G. Zhu, Anal. Chim. Acta 564 (2006) 243–247.
[16] H. Yang, M. Yoshio, K. Isono, R. Kuramoto, Electrochem. Solid-State Lett. 5 (2002) A141–A144.
[17] M. Endo, Y.J. Kim, K. Osawa, K. Ishii, T. Inoue, T. Nomura, N. Miyashita, M.S. Dresselhaus, Electrochem. Solid-State Lett. 6 (2003) A23–A26.
[18] S.R.S. Prabaharan, R. Vimala, Z. Zainal, J. Power Sources 161 (2006) 730–736.
[19] E. Frackowiak, F. Béguin, Carbon 39 (2001) 937–950.
[20] M. Toupin, D. Bélanger, I.R. Hill, D. Quinn, J. Power Sources 140 (2005) 203–210.
[21] A.G. Pandolfo, A.F. Hollenkamp, J. Power Sources 157 (2006) 11–27.
[22] H. Liu, C. Song, L. Zhang, J. Zhang, H. Wang, D.P. Wilkinson, J. Power Sources 155 (2006) 95–110.
[23] N.R. Elezović, B.M. Babić, Lj.M. Vračar, N.V. Krstajić, J. Serb. Chem. Soc. 72 (2007) 699–708.
[24] G.A. Snook, N.W. Duffy, A.G. Pandolfo, J. Power Sources 168 (2007) 513–521.
[25] Z. Liu, L. Hong, S.W. Tay, Mater. Chem. Phys. 105 (2007) 222–228.
[26] D. He, L. Yang, S. Kuang, Q. Cai, Electrochem. Commun. 9 (2007) 2467–2472.
[27] L.T. Markovska, V.D. Meshko, M.S. Marinkovski, J. Serb. Chem. Soc. 71 (2006) 957–967.
[28] F. Zaragoza-Martín, D. Sopeña-Escario, E. Morallón, C. Salinas-Martínez de Lecea, J. Power Sources 171 (2007) 302–309.
[29] E.P. Maris, R.J. Davis, J. Catalysis 249 (2007) 328–337.
[30] P. Paunovic, O. Popovski, S. Hadzi-Jordanov, A. Dimitrov, D. Slavkov, J. Serb. Chem. Soc. 71 (2006) 149–165.
[31] R. Richner, S. Moeller, A. Wokaum, Carbon 40 (2002) 307–314.
[32] V. Panić, T. Vidaković, S. Gojković, A. Dekanski, S. Milonjić, B. Nikolić, Electrochim. Acta 48 (2003) 3805–3813.
[33] D. Qu, H. Shi, J. Power Sources 74 (1998) 99–107.
[34] J. Gamby, P.L. Taberna, P. Simon, J.F. Fauvarque, M. Chesneau, J. Power Sources 101 (2001) 109–116.
[35] C. Lin, J.A. Ritter, B.N. Popov, J. Electrochem. Soc. 146 (1999) 3639–3643.
[36] H. Shi, Electrochim. Acta 41 (1996) 1633–1639.
[37] G. Salitra, A. Soffer, L. Eliad, Y. Cohen, D. Aurbach, J. Electrochem. Soc. 147 (2000) 2486–2493.
[38] S.-I. Pyun, C.-H. Kim, S.-W. Kim, J.-H. Kim, J. New Mat. Electrochem. Syst. 5 (2002) 289–295.
[39] C. Lin, B.N. Popov, H.J. Ploehn, J. Electrochem. Soc. 149 (2002) A167–A175.
[40] M. Ramani, B. Haran, R. White, B. Popov, J. Electrochem. Soc. 148 (2001) A374–A380.
[41] J. Zhang, D. Jiang, B. Chen, J. Zhu, L. Jiang, H. Fang, J. Electrochem. Soc. 148 (2001) A1362–A1367.
[42] J.H. Park, O.O. Park, J. Power Sources 109 (2002) 121–126.
[43] C.-C. Hu, W.-C. Chen, Electrochim. Acta 49 (2004) 3469–3477.
[44] W.-C. Chen, C.-C. Hu, C.-C. Wang, C.-K. Min, J. Power Sources 125 (2004) 292–298.
[45] M.S. Dandekar, G. Arabale, K. Vijayamohanan, J. Power Sources 141 (2005) 198–203.
[46] V. Panić, A. Dekanski, S. Gojković, V. Mišković-Stanković, B. Nikolić, Mater. Sci. Forum 453–454 (2004) 133–138.
[47] V. Panić, A. Dekanski, S. Gojković, S. Milonjić, V.B. Mišković-Stanković, B. Nikolić, Mater. Sci. Forum 494 (2005) 235–240.
[48] F. Raimondi, G.G. Scherer, R. Kötz, A. Wokaun, Angew. Chem. Int. Ed. 44 (2005) 2190–2209.
[49] P.L. Taberna, C. Portet, P. Simon, Appl. Phys. A 82 (2006) 639–646.
[50] M. Arulepp, J. Leis, M. Lätt, F. Miller, K. Rumma, E. Lust, A.F. Burke, J. Power Sources 162 (2006) 1460–1466.
[51] D. Johnson, Z. View® Sofware, Copyright ©1990–2002 Scribner Associates, Inc. (www.scribner.com).
[52] A. Braun, J. Kohlbrecher, M. Bärtsch, B. Schnyder, R. Kötz, O. Haas, A. Wokaun, Electrochim. Acta 49 (2004) 1105–1112.
[53] J. Maruyama, I. Abe, Electrochim. Acta 46 (2001) 3381–3386.
[54] M.G. Sullivan, R. Kötz, O. Haas, J. Electrochem. Soc. 147 (2000) 308–317.
[55] A. Dekanski, J. Stevanović, R. Stevanović, B.Ž. Nikolić, V.M. Jovanović, Carbon 39 (2001) 1195–1205.
[56] K. Kinoshita, J.A.S. Bett, Carbon 12 (1974) 525–533.
[57] S. Ardizzone, G. Fregonara, S. Trasatti, Electrochim. Acta 35 (1990) 263–267.
[58] X. Wang, H. Zhang, J. Zhang, H. Xu, X. Zhu, J. Chen, B. Yi, J. Power Sources 162 (2006) 474–479.
[59] W.H. Mulder, J.H. Sluytes, T. Pajkossy, I. Nyikos, J. Electroanal. Chem. 285 (1990) 103–115.